

---

# SEGA: A Transferable Signed Ensemble Gaussian Black-Box Attack against No-Reference Image Quality Assessment Models

---

**Yujia Liu\***

NERCVT, School of Computer Science, Peking University, China

National Key Laboratory for Multimedia Information Processing, Peking University, China

School of Mathematical Sciences, Peking University, China

yujia\_liu@pku.edu.cn

**Dingquan Li**

Peng Cheng Laboratory

China

dingquanli@pku.edu.cn

**Tiejun Huang**

NERCVT, School of Computer Science, Peking University, China

National Key Laboratory for Multimedia Information Processing, Peking University, China

School of Mathematical Sciences, Peking University, China

tjhuang@pku.edu.cn

## Abstract

No-Reference Image Quality Assessment (NR-IQA) models play an important role in various real-world applications. Recently, adversarial attacks against NR-IQA models have attracted increasing attention, as they provide valuable insights for revealing model vulnerabilities and guiding robust system design. Some effective attacks have been proposed against NR-IQA models in white-box settings, where the attacker has full access to the target model. However, these attacks often suffer from poor transferability to unknown target models in more realistic black-box scenarios, where the target model is inaccessible. This work makes the first attempt to address the challenge of low transferability in attacking NR-IQA models by proposing a transferable Signed Ensemble Gaussian black-box Attack (SEGA). The main idea is to approximate the gradient of the target model by applying Gaussian smoothing to source models and ensembling their smoothed gradients. To ensure the imperceptibility of adversarial perturbations, SEGA further removes inappropriate perturbations using a specially designed perturbation filter mask. Experimental results on the CLIVE dataset demonstrate the superior transferability of SEGA, validating its effectiveness in enabling successful transfer-based black-box attacks against NR-IQA models.

## 1 Introduction

Image Quality Assessment (IQA) models, which predict quality scores for input images, play an important role in various downstream tasks. For instance, the predicted scores can serve as a key factor in recommendation systems [1]. In addition, they are often used to guide model optimization

---

\*corresponding author

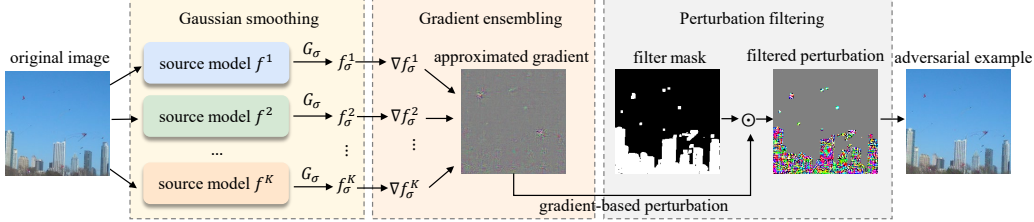


Figure 1: Overview of the proposed SEGA method. SEGA leverages ensembled gradients from multiple source models with Gaussian smoothing to approximate the gradient of the target model. To enhance the imperceptibility of adversarial perturbations, SEGA designs a perturbation filter mask to remove inappropriate perturbations.

and performance evaluation in domains such as medical diagnosis [2] and autonomous driving [3]. Based on the availability of reference images, IQA can be categorized into Full-Reference IQA (FR-IQA) and No-Reference IQA (NR-IQA). FR-IQA models assess the quality of distorted images with corresponding reference images [4, 5], whereas NR-IQA models predict quality scores without any reference [6, 7]. This paper focuses on NR-IQA, which poses greater challenges and is commonly used in practical real-world applications [8].

With the widespread deployment of NR-IQA models in various downstream applications, adversarial attacks targeting these models have attracted increasing attention [9–11]. Such attacks aim to mislead predicted quality scores by introducing imperceptible perturbations to input images, thereby exposing potential vulnerabilities in NR-IQA models that may pose serious security risks in real-world scenarios. For example, if an NR-IQA model assigns a high-quality score to a low-quality image under attack, it may mislead recommendation systems into promoting poor-quality content, resulting in a degraded user experience [12, 13]. In more critical domains such as healthcare, the misjudgment of low-quality medical images could severely compromise diagnostic outcomes [14]. Therefore, investigating adversarial attacks against NR-IQA models is essential for identifying their weaknesses and guiding the development of more robust and trustworthy systems.

Recent studies primarily focus on attacking NR-IQA models in white-box scenarios, where full access to the target model is available. White-box attacks typically generate adversarial perturbations based on the gradient of the input image [9, 10, 15, 16], as it indicates the direction in which prediction scores change most rapidly. For instance, Shumitskaya *et al.* [15] proposed a universal perturbation by aggregating the gradients across the entire test set with weighted summation, effectively increasing the predicted scores for most inputs. In contrast, Zhang *et al.* [9] formulated an optimization problem for individual images with Lagrange multipliers and solved it using gradient descent methods, achieving significant errors in prediction consistency across a dataset.

However, research on attacking NR-IQA models in the more challenging black-box scenario remains limited. In this setting, adversarial perturbations are generated solely based on input-output pairs, without access to the model’s internal information. Yang *et al.* [11] proposed a query-based method that iteratively queries the target model and performs a binary search in the polar space to locate effective perturbations. While effective at inducing prediction errors, this approach is highly time-consuming due to the need for thousands of queries. An alternative strategy is transfer-based black-box attacks, where attackers generate adversarial examples using accessible source models and then transfer them to the target model. However, existing attacks on NR-IQA models have demonstrated limited transferability to unknown target models [9, 17], and to date, no attack method with good transferability for NR-IQA tasks has been proposed.

In this paper, we propose a black-box attack method against NR-IQA models that achieves strong transferability. The main idea is to approximate the gradients of the target model using accessible source models while maintaining the imperceptibility of adversarial perturbations. Existing white-box attacks [9, 15] have highlighted the importance of gradients, which reveal the direction of the steepest change in prediction scores. Given that different NR-IQA models are designed to solve the same task, it is reasonable to assume that they share similar gradient behaviors. However, previous studies have shown that raw gradients often contain significant noises [18, 19], which may lead to inconsistencies between the gradients of the source and target models, and thereby reduce the transferability of

adversarial examples. To address this, we aim to remove noises in the source model gradients to better approximate the target model’s gradient directions.

In detail, we propose the Signed Ensemble Gaussian Attack (SEGA) method on NR-IQA models, which consists of three steps: Gaussian smoothing, gradient ensembling, and perturbation filtering (as shown in Fig. 1). The first two steps aim to improve gradient approximation, while the final step enhances the imperceptibility of the resulting perturbations. Given an input image and a source model, we first apply Gaussian smoothing to the model and use the gradient of the smoothed output as an approximation. This is because smoothed gradients can effectively reduce noises in the original gradient [18]. Next, inspired by advances in transfer-based attacks for classification models [20], we employ an ensemble of smoothed source models to further refine the gradient approximation and improve transferability. The adversarial perturbation is then generated by taking the sign of the approximated gradient scaled by a small step size. Finally, to improve the imperceptibility of adversarial perturbations, we design a perturbation filter mask that removes inappropriate perturbations while maintaining the attack effectiveness.

The main contributions of this work are as follows. (1) Methodologically, we propose SEGA—the first transfer-based black-box attack method specifically designed for NR-IQA models. SEGA introduces Gaussian smoothing into the adversarial attack framework for the first time, enabling a more accurate approximation of target model gradients. (2) Theoretically, we analyze the upper bound on the error between the approximated gradient obtained from source models and the true gradient of the target model, providing insights into the effectiveness of gradient smoothing and ensembling. (3) Empirically, extensive experiments on the CLIVE dataset [21] demonstrate that SEGA significantly enhances the transferability of adversarial examples across NR-IQA models, as evaluated by both prediction accuracy and score consistency.

## 2 Related Works

### 2.1 White-Box Attacks Against NR-IQA Models

Several studies have explored white-box attacks on NR-IQA models and achieved impressive attack performance with the use of input image gradients. Zhang *et al.* [9] proposed the perceptual attack by formulating it as an optimization problem with Lagrange multipliers, which they solved using gradient descent. This approach significantly reduced prediction accuracy and caused prediction errors. Shumitskaya *et al.* [15] proposed a universal perturbation method that generates adversarial perturbations by computing a weighted sum of image gradients across the test dataset. The resulting perturbation can effectively increase the predicted scores for most inputs. Meanwhile, Liu *et al.* [17] directly adapted the classical FGSM attack [22], which uses the sign of gradients, from image classification to NR-IQA models. Recently, the IOI attack was proposed, which post-processed adversarial examples generated by FGSM in the frequency domain to improve the imperceptibility of perturbations [16]. These works highlight the important role of gradients in attack methods and demonstrate the vulnerability of NR-IQA models to white-box adversarial attacks.

### 2.2 Black-Box Attacks Against NR-IQA Models

Black-box attacks on NR-IQA models have been relatively underexplored. There are two main strategies for attacking models in the black-box scenario. One is the query-based approach, where attackers can query the target model multiple times to approximate the gradient, which is then used to optimize the perturbations and generate adversarial examples. Yang *et al.* [11] adapted the approach from SurFree [23], employing binary search in polar coordinates to generate adversarial examples by continuously querying the changes in predicted scores. Yu [24] developed a query-based attack based on a random search paradigm. Although query-based attacks can achieve impressive attack performance in black-box scenarios, they require a large number of queries (nearly 10,000 times [11, 24]) to generate a single adversarial example, making the process highly time-consuming.

Compared to query-based attacks, transfer-based approaches are more efficient. Transfer-based attacks have been widely studied in the context of classification model attacks [25, 26], but remain largely unexplored for NR-IQA models. Existing adversarial attacks on NR-IQA often suffer from poor transferability across different models [9, 24]. Korhonen *et al.* [27] attributed this issue to the diverse features learned by different NR-IQA models. To address this, they re-trained a ResNet-based

source model [28] to capture more generic quality assessment features. While adversarial examples generated from this model some marginal improvements in transferability, the gains were limited. Moreover, re-training the source model causes considerable computational overhead.

### 3 Method

In this paper, we propose a transfer-based black-box attack method against NR-IQA models, named Signed Ensemble Gaussian Attack (SEGA). SEGA consists of three components: Gaussian smoothing (Sec. 3.2), gradient ensembling (Sec. 3.3), and perturbation filtering (Sec. 3.4), as illustrated in Fig. 1. The first two parts aim to reduce noise in the gradients and accurately approximate the gradients of the target model. Perturbation filtering focuses on enhancing the perturbations’ imperceptibility to ensure that adversarial examples are perceptually similar to the original images.

#### 3.1 Problem Definition

In the transfer-based black-box scenario, there is an unknown NR-IQA target model  $h$  and an available source model  $f$ . Given an input image  $x$ , the objective is to design an adversarial perturbation based on the source model  $f$ , denoted as  $\Delta x(f)$ , that maximally manipulates the prediction score of  $x + \Delta x(f)$  by  $h$ . Meanwhile, the adversarial image  $x + \Delta x(f)$  should maintain perceptual similarity to the original image  $x$ , ensuring that both images receive the same objective score from human observers, *i.e.*

$$\max_{\Delta x(f)} |h(x + \Delta x(f)) - h(x)| \quad \text{s.t. } D(x, x + \Delta x(f)) \leq \epsilon, \quad (1)$$

where  $D(\cdot, \cdot)$  measures the perceptual distance between the original image and the adversarial example, and  $\epsilon$  represents a predefined threshold. In this paper, we define  $D(x, x + \Delta x(f)) = \|\Delta x(f)\|_\infty$  with the  $\ell_\infty$  function commonly used in previous studies [22, 17, 16]. In the following text, we use  $\Delta x$  instead of  $\Delta x(f)$  for its simplicity.

Since the input gradient of the target model is inaccessible, the perturbation  $\Delta x$  is crafted by solving the following white-box optimization problem on the accessible source model  $f$ :

$$\max_{\Delta x} |f(x + \Delta x) - f(x)| \quad \text{s.t. } \|\Delta x\|_\infty \leq \epsilon. \quad (2)$$

This white-box problem has been widely explored [9, 15, 22]. Due to the computational efficiency, we adopt the idea from FGSM [22] attack to solve Eq. (2), *i.e.*

$$\Delta x = \epsilon \cdot \text{sgn}(\nabla f(x)), \quad (3)$$

where  $\text{sgn}(\cdot)$  denotes the sign function, and  $\nabla f(x)$  is the gradient of the source model  $f$  with respect to the input image  $x$ .

#### 3.2 Gaussian Smoothing

According to Eq. (3), the transferability of  $x + \Delta x$  from the source model  $f$  to the target model  $h$  primarily depends on the extent of  $h$ ’s instability along the direction of  $\text{sgn}(\nabla f(x))$ . While the level sets of models within the same task are expected to exhibit global similarity [29, 30], local fluctuations caused by noise [18] in  $\nabla f(x)$  may hurt this similarity. An efficient way to remove noise in  $\nabla f(x)$  is smoothing  $f$  with a Gaussian mollifier [18], *i.e.*

$$f_\sigma(x) = \frac{1}{(2\pi)^{d/2}} \int_{\mathbb{R}^d} f(x + \sigma u) e^{-\|u\|_2^2/2} du = \mathbb{E}_{u \sim \mathcal{N}(0, I_d)} [f(x + \sigma u)]. \quad (4)$$

In this formula,  $d$  denotes the dimension of the image  $x$ ,  $\mathcal{N}(0, I_d)$  is the  $d$ -dimensional standard normal distribution with  $I_d$  as the identity matrix, and  $\sigma > 0$  determines the standard deviation of the term  $\sigma u$ . Additionally,  $\sigma$  controls the degree of smoothing. Larger  $\sigma$  values result in a smoother approximation, while smaller  $\sigma$  values preserve more details of the model  $f$  [31]. Theorem 1 illustrates this point and the proof is provided in Appendix A.

**Theorem 1** Suppose  $f$  is Lipschitz-continuous, and  $f_\sigma$  is the Gaussian smoothing of  $f$ . Then, for every  $x$ , we have

$$\lim_{\sigma \rightarrow 0} f_\sigma(x) = f(x). \quad (5)$$

According to Eq. (4), we define

$$f_\sigma(x) = \frac{1}{m} \sum_{i=1}^m f(x + \sigma u_i), \quad \text{where } u_i \sim \mathcal{N}(0, I_d), \quad (6)$$

as the discrete Gaussian-smoothed version of  $f$ , where  $m$  is the number of samples. The gradient  $\nabla f(x)$  is then substituted by  $\nabla f_\sigma(x)$ , *i.e.*

$$\nabla f(x) \approx \nabla f_\sigma(x) = \frac{1}{m} \sum_{i=1}^m \nabla f(x + \sigma u_i). \quad (7)$$

### 3.3 Gradient Ensembling

Ensembling source models to generate more transferable adversarial examples is a commonly used strategy in image classification tasks [20, 32, 26]. This approach is often considered a form of model augmentation, where multiple source models are attacked simultaneously.

Inspired by this idea, we ensemble the gradients of  $K$  source models  $\{f^1, \dots, f^K\}$  to further reduce the noise present in the gradient of any single source model. Since every source model is smoothed by a Gaussian function, the final ensembled gradient with smoothing is

$$\hat{g}(x) = \frac{1}{K} \sum_{k=1}^K \nabla f_\sigma^k(x) = \frac{1}{K \cdot m} \sum_{k=1}^K \sum_{i=1}^m \nabla f^k(x + \sigma u_i^k), \quad (8)$$

where  $u_i^k \in \mathbb{R}^d$  and  $u_i^k \sim \mathcal{N}(0, I_d)$ . The following theorem shows that there is an upper bound on the approximation error between  $\hat{g}(x)$  and the gradient  $\nabla h(x)$  of the target model  $h$ . Due to the space limitation, the proof of the theorem is provided in Appendix B.

**Theorem 2** *Suppose the gradient of the target model  $h$  is  $L$ -Lipschitz with  $L$  being the Lipschitz constant, and  $\hat{g}(x)$  is defined in Eq. (8), we have*

$$\|\hat{g}(x) - \nabla h(x)\| \leq \left( L\sigma + \frac{C}{\sigma} \right) \sqrt{2} \frac{\Gamma(\frac{d+1}{2})}{\Gamma(\frac{d}{2})}, \quad (9)$$

where  $C$  is a constant related to  $\{f^1, \dots, f^K\}$  and  $\Gamma(\cdot)$  represents the Gamma function [33].

### 3.4 Perturbation Filtering

Based on Eq. (8) and the basic idea of the FGSM attack [22], the adversarial perturbation is

$$\Delta x = \epsilon \cdot \text{sgn}(\hat{g}(x)). \quad (10)$$

However, we think this straightforward approach may introduce redundant noises, resulting in poor imperceptibility of the adversarial perturbations.

Firstly, we observe that the  $\text{sgn}(\cdot)$  function may amplify some **unimportant components** in the gradient  $\hat{g}(x)$ . In detail, components with small absolute values in  $\hat{g}(x)$  theoretically have limited impact on the predicted score, yet the  $\text{sgn}(\cdot)$  function treats them as equally important as those with larger values. For instance, if a component of  $\hat{g}(x)$  is 0.0001, adding perturbations to it has little impact on the predicted score. However, since  $\text{sgn}(0.0001) = 1$ , Eq. (10) still applies an  $\epsilon$ -sized perturbation to this component. Therefore, to remove such kinds of unimportant perturbations, we design a filter mask based on the component values of  $\hat{g}$  as follows where  $\alpha$  is a pre-defined threshold.

$$M_j^F = \begin{cases} 0, & \text{if } \hat{g}_j < \alpha, \\ 1, & \text{otherwise.} \end{cases} \quad (11)$$

In this equation,  $j \in \{1, \dots, d\}$  denotes the index of each component.

Secondly, recognizing that different regions of an image exhibit varying tolerance to perturbations [34], we further remove some **inappropriate perturbations** based on a Just Noticeable Difference (JND) map. Studies have shown that perturbations in low-frequency regions are more perceptible compared

to those in high-frequency regions [35, 11]. The JND value at each pixel serves as a metric to quantify this tolerance. It represents the maximum perturbation that the pixel can tolerate without being perceptible. Therefore, we compute the JND map of  $x$  using the method proposed by Liu *et al.* [35], and design a mask based on  $\text{JND}(x)$  as follows,

$$M_j^{\text{JND}} = \begin{cases} 0, & \text{if } \text{JND}_j(x) < \epsilon, \\ 1, & \text{otherwise.} \end{cases} \quad (12)$$

The final filtered adversarial perturbation is then defined as:

$$\Delta x = (M^{\text{JND}} \odot M^{\mathcal{F}}) \odot (\epsilon \cdot \text{sgn}(\hat{g}(x))), \quad (13)$$

where  $\odot$  represents the element-wise (Hadamard) multiplication. The complete SEGA algorithm is provided in Appendix C.

## 4 Experiments

In this section, we first introduce experimental settings (Sec.4.1), including the compared NR-IQA attack methods, the transfer-based black-box settings, and the hyperparameters of attacks. Next, we report the superior transferability of SEGA compared to existing attacks in Sec.4.2. We also demonstrate the imperceptibility of the perturbations using both quantitative and qualitative metrics (Sec.4.3). Finally, Sec.4.4 presents ablation studies to justify the choice of hyperparameters in SEGA. Due to space limitations, additional explorations are provided in the appendix, including training details of NR-IQA models (Appendix D), some ablation studies (Appendix G), the effectiveness of SEGA against robustly trained models (Appendix H) and the comparison of SEGA with query-based black-box attacks (Appendix I).

### 4.1 Experimental Settings

**Compared attack methods.** We compare our method with five NR-IQA attack methods: FGSM adapted for NR-IQA models [17], perceptual attack (Pattack) [9], OUAP [15], IOI [16] and the attack proposed by Korhonen *et al.* [27] (short for Kor). All these methods are applicable in the transfer-based scenario.

**Transfer-based black-box settings.** We conduct extensive experiments on the CLIVE dataset [21] whose 20% is randomly chosen for testing. Four state-of-the-art (SOTA) NR-IQA models: Hyper-IQA [36], DBCNN [7], LinearityIQA [37], and LIQE [38] are used in this paper. Each of these models is individually taken as the target model  $h$ . For the proposed SEGA method, the remaining three models are used as an ensemble of source models  $\{f^1, f^2, f^3\}$ . The Kor method uses a pre-trained ResNet model as the source model regardless of the target model [27]. For other methods, each of the other three models is independently used as the source model. We evaluate the attack performance for each  $\{f^k, h\}$  pair ( $k = 1, 2, 3$ ) and report the best performance. Additionally, we explore a simple ensemble strategy for these methods by averaging adversarial examples generated against all source models, with results provided in Appendix F.

**Parameters chosen.** Following the setups from existing works, we configure each attack method as follows. We use the one-step FGSM attack with an attack strength of 0.03 [17]. Pattack [4] employs LPIPS as the constraint, with a weight of 9,000,000 [11]. OUAP generates adversarial examples using 10 iterations with an attack strength of 0.03 [15]. IOI uses a learning rate of 0.1 and a truncation parameter of 0.07 [16]. For the Kor attack, the learning rate is set to 2. The proposed SEGA method sets the attack strength to  $\epsilon = 0.03$ . For Gaussian smoothing, the sample number is  $m = 10$ , and the smoothing parameter is  $\sigma = 10/255$ . The filter mask  $M^{\mathcal{F}}$  uses a threshold of  $\alpha = 0.02$ .

### 4.2 Comparison in Transferability

In this section, we evaluate the transferability of SEGA in comparison with SOTA attack methods. Transferability is assessed using five metrics calculated between predicted scores before and after attacks: Mean Absolute Error (MAE), R robustness [9], Spearman Rank Order Correlation Coefficient (SROCC), Pearson’s Linear Correlation Coefficient (PLCC), and Kendall’s Rank-Order Correlation Coefficient (KROCC). Higher MAE and lower values for the other metrics indicate better transferability. The main results are shown in Table 1.

Table 1: Comparison of SEGA with other attacks. For FGSM, Pattack, OUAP, and IOI, we report their best performance across all source models, with the corresponding source model indicated in the ‘best source’ column. The highest performance values are highlighted in **bold**

Target: HyperIQA							Target: DBCNN						
source	MAE $\uparrow$	R $\downarrow$	SROCC $\downarrow$	PLCC $\downarrow$	KROCC $\downarrow$	source	MAE $\uparrow$	R $\downarrow$	SROCC $\downarrow$	PLCC $\downarrow$	KROCC $\downarrow$		
FGSM	DBCNN	8.648	1.054	0.825	0.841	0.640	LIQE	7.950	1.003	0.866	0.859	0.680	
Pattack	Linearity	7.992	1.153	0.941	0.923	0.793	Linearity	6.423	1.148	0.968	0.966	0.852	
OUAP	Linearity	<b>16.779</b>	0.850	0.733	<b>0.692</b>	0.552	LIQE	<b>13.282</b>	0.894	0.747	0.731	0.557	
IOI	Linearity	7.728	1.120	0.931	0.921	0.781	Linearity	5.974	1.262	0.931	0.912	0.770	
Kor	-	16.505	<b>0.781</b>	0.858	0.842	0.675	-	8.914	1.028	0.883	0.869	0.710	
SEGA	-	12.186	0.883	<b>0.675</b>	0.706	<b>0.507</b>	-	10.493	<b>0.876</b>	<b>0.562</b>	<b>0.626</b>	<b>0.412</b>	
Target: LinearityIQA							Target: LIQE						
source	MAE $\uparrow$	R $\downarrow$	SROCC $\downarrow$	PLCC $\downarrow$	KROCC $\downarrow$	source	MAE $\uparrow$	R $\downarrow$	SROCC $\downarrow$	PLCC $\downarrow$	KROCC $\downarrow$		
FGSM	HyperIQA	12.383	0.969	0.709	0.666	0.531	HyperIQA	11.344	1.103	0.909	0.894	0.754	
Pattack	HyperIQA	7.896	1.156	0.953	0.930	0.824	HyperIQA	6.145	1.440	0.976	0.979	0.876	
OUAP	DBCNN	15.789	0.966	0.663	0.596	0.5010	DBCNN	6.406	1.450	0.938	0.941	0.826	
IOI	HyperIQA	9.133	1.123	0.870	0.865	0.6932	HyperIQA	7.098	1.437	0.956	0.948	0.837	
Kor	-	14.475	0.913	0.8020	0.786	0.612	-	10.742	1.311	0.899	0.883	0.752	
SEGA	-	<b>17.938</b>	<b>0.700</b>	<b>0.504</b>	<b>0.503</b>	<b>0.366</b>	-	<b>15.094</b>	<b>0.927</b>	<b>0.831</b>	<b>0.801</b>	<b>0.663</b>	

Table 2: Quantitative comparison of the image quality of adversarial examples generated by different attack methods against various target models, with SSIM ( $\uparrow$ ) values computed between the adversarial examples and the original images.

Target	HyperIQA	DBCNN	LinearityIQA	LIQE
FGSM	0.733	0.755	0.740	0.740
Pattack	0.731	0.731	0.733	0.733
OUAP	0.815	0.803	0.826	0.826
IOI	0.883	0.883	0.888	0.888
Kor	0.931	0.931	0.931	0.931
SEGA	0.862	0.857	0.881	0.863

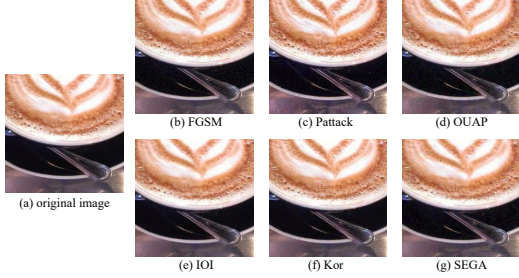


Figure 2: Visualization of adversarial examples generated by different attack methods against the target HyperIQA model. Please zoom in for a clearer view.

As shown in the table, SEGA outperforms other methods across nearly all metrics and target models, particularly in SROCC, PLCC, and KROCC. In every case, SEGA achieves the lowest SROCC after attacks, indicating its superior ability to disrupt prediction consistency compared to other methods. For instance, when attacking DBCNN, SEGA achieves an SROCC of 0.56, whereas the second-best method (OUAP) achieves only around 0.75. In contrast, the other methods exhibit weak attack performance across most metrics. When attacking DBCNN, the MAE values for compared methods except OUAP are all below 10, and their SROCC values remain above 0.85, highlighting their poor transferability from source models to the target model. When the target model is LinearityIQA or LIQE, SEGA achieves the best attack performance in terms of both MAE and R robustness, demonstrating its strong capability to manipulate prediction accuracy.

There are some exceptions in Table 1 where SEGA does not outperform existing methods, particularly in comparisons with OUAP. We attribute this to the relatively noticeable perturbations produced by OUAP, as discussed in the next section. Additionally, while SEGA’s perturbation filtering enhances imperceptibility by removing certain noise, it may slightly reduce attack effectiveness.

### 4.3 Imperceptibility of Adversarial Perturbations

Since the imperceptibility of adversarial perturbations is a crucial requirement for attacks, we provide both quantitative and qualitative comparisons in this section.

The average SSIM [39] values between adversarial examples and the original input images are reported in Table 2. Higher SSIM values indicate greater similarity between adversarial examples

Table 3: Ablation studies on the impact of Gaussian smoothing and gradient ensembling on transferability.

Gauss.	Ens.	MAE↑	R↓	SROCC↓	PLCC↓	KROCC↓
✗	✗	7.003	1.119	0.836	0.849	0.655
✗	✓	7.848	1.049	0.786	0.802	0.604
✓	✗	9.134	0.976	0.670	0.730	0.500
✓	✓	<b>10.387</b>	<b>0.882</b>	<b>0.571</b>	<b>0.642</b>	<b>0.423</b>

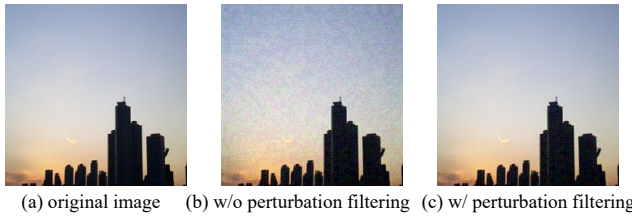


Figure 3: A visualization result of adversarial examples generated with and without the use of perturbation filtering.

Table 4: Ablation studies on the impact of perturbation filtering on the imperceptibility of adversarial perturbations.

$M^F$	$M^{JND}$	$\ell_\infty \downarrow$	$\ell_1 \downarrow$	SSIM ↑	LPIPS ↓	DISTS ↓
✗	✗	8.0	7.838	0.749	0.314	0.202
✗	✓	8.0	5.511	0.808	0.290	0.188
✓	✗	8.0	6.501	0.817	0.261	0.181
✓	✓	8.0	4.538	0.857	0.235	0.167

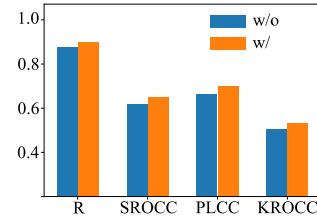


Figure 4: The effect of perturbation filtering on transferability.

and the original images, suggesting that the adversarial perturbations are less perceptible. Additional metrics for quantitative comparison are provided in Appendix E. From Table 2, we observe that SEGA method demonstrates significantly better imperceptibility compared to FGSM, Pattack, and OUAP. Furthermore, SEGA achieves imperceptibility comparable to that of IOI and the Kor attack across all target models. For instance, when HyperIQA is the target model, the SSIM value of SEGA is only 0.02 lower than that of IOI but exceeds those of FGSM and Pattack by more than 0.12.

To provide a more intuitive comparison of the imperceptibility of these attacks, we present a visualization result in Fig. 2. Additionally, more qualitative results are included in Appendix E. From Fig. 2, it is evident that adversarial perturbations in the examples generated by SEGA are less perceptible compared to those generated by FGSM and OUAP. Although SEGA falls slightly behind IOI and the Kor attack in SSIM values, the adversarial examples generated by these methods appear perceptually similar to the human visual system.

#### 4.4 Ablation Studies

In this section, we conduct ablation studies on the three components of SEGA: Gaussian smoothing, gradient ensembling, and perturbation filtering. First, we explore the effectiveness of the first two components on transferability as well as the parameters chosen for these parts. Then, we evaluate the impact of the perturbation filtering on imperceptibility and transferability. All experiments in this section attack the DBCNN as the target model.

**Effectiveness of Gaussian smoothing and gradient ensembling.** Table 3 presents the ablation study on Gaussian smoothing and gradient ensembling. In the table, “Gauss.(✗)” indicates that for a source model  $f$ , the gradient  $\nabla f(x)$  is directly used to guide the generation of adversarial examples, instead of using the gradient of the Gaussian-smoothed function. And “Ens.(✗)” denotes that only HyperIQA is used as the source model, instead of the full set of source models {HyperIQA, LinearityIQA, LIQE}. Table 3 demonstrates that both components contribute to improving the transferability of adversarial examples, with their combination yielding the best results. Furthermore, Gaussian smoothing proves to be more effective than gradient ensembling in enhancing transferability.

**Effectiveness of perturbation filtering.** Table 4 presents ablation studies evaluating the impact of the filter mask  $M^F$  and the JND mask  $M^{JND}$  on the imperceptibility of adversarial perturbations. The evaluation metrics include the  $\ell_\infty$  and  $\ell_1$  norms of the perturbations, along with widely used perceptual metrics—SSIM, LPIPS, and DISTS [5]—calculated between the adversarial examples and the corresponding original images. The results demonstrate that both masks substantially enhance the imperceptibility of perturbations. Fig. 3 provides a visual example illustrating the combined effect of both masks. We further analyze the impact of perturbation filtering on transferability in Fig. 4. Since

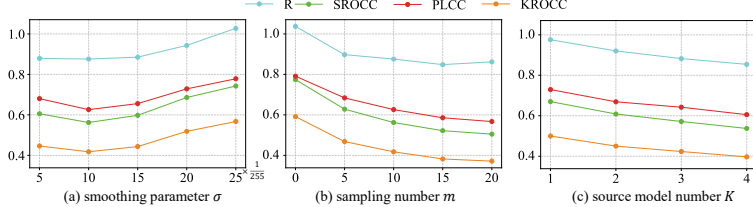


Figure 5: Analysis of hyper-parameter ablation studies and the impact of perturbation filtering on transferability.

Table 5: Complexity and efficiency comparison.

attack	forward	time (s)
FGSM	1	0.087
Patatck	200	9.337
OUAP	10	0.427
IOI	1	0.043
Kor	20	18.682
SEGA	30	1.309

filtering removes certain perturbation components, a slight reduction in transferability is observed compared to the unfiltered case. However, we consider this reduction acceptable given the substantial improvement in imperceptibility. For example, the robustness score  $R$  differs by only approximately 0.02 with and without filtering. These findings highlight the necessity of incorporating perturbation filtering in SEGA, which slightly reduces transferability but significantly enhances the image quality of adversarial examples.

**The smoothing parameter  $\sigma$  in Gaussian smoothing.** Fig. 5 (a) illustrates the impact of the smoothing parameter  $\sigma$  on transferability. The results indicate that transferability initially improves but then declines as  $\sigma$  increases. For instance, the PLCC value decreases from approximately 0.7 to 0.6 as  $\sigma$  increases from 5/255 to 10/255, and then rises to nearly 0.8 as  $\sigma$  increases to 25/255. Similar trends also occur on other metrics. This phenomenon suggests that  $\sigma$  represents a trade-off between smoothness and transferability. On one hand, smaller  $\sigma$  limits the effectiveness of noise removal and thus reduces transferability. On the other hand, larger  $\sigma$  results in broader smoothing of  $f$ , which may introduce large approximation errors. As a result,  $f_\sigma$  may no longer serve as a good approximation of the target model. In our main experiments, we select  $\sigma = 10/255$ .

**The sampling number  $m$  in Gaussian smoothing.** Since explicitly calculating the gradient of  $f_\sigma$  is challenging, we instead use the expectation as shown in Eq. (7). The number of sampling points,  $m$ , determines the accuracy of approximating  $\nabla f_\sigma(x)$  by the empirical mean  $\frac{1}{m} \sum_{i=1}^m \nabla f(x + \sigma u_i)$ . The ablation study results for  $m$  are presented in Fig. 5 (b). It is evident that transferability improves as  $m$  increases. Notably, when  $m$  reaches 20, the KROCC value drops below 0.4, indicating that larger  $m$  effectively reduces noise in the gradients and enhances transferability. However, since a larger  $m$  may lead to inefficiency due to the increased sampling complexity (as analyzed in Sec. 4.5), we select  $m = 10$  in this paper. Nevertheless, using a larger  $m$ , such as 20, could be a reasonable choice if better transferability is needed and some computational cost can be accommodated.

**The number  $K$  of source models in gradient ensembling.** We evaluate how transferability changes as the number of source models increases. Specifically, we add MANIQA [6] to the source model set and incrementally include NR-IQA models as source models following the order of HyperIQA, LinearityIQA, LIQE, and MANIQA, calculating the ensemble gradient using Eq. (8). The results are presented in Fig. 5 (c). It is evident that incorporating more source models into the ensemble improves transferability. This finding suggests that using as many source models as possible can be beneficial when attacking unknown target models in real-world applications.

## 4.5 Computational Complexity and Efficiency

In this subsection, we compare the computational complexity and efficiency of SEGA with other attack methods to demonstrate that SEGA is still an efficient attack method despite utilizing Gaussian sampling and ensembled source models. The computational complexity is assessed based on the number of forward propagations required to generate a single adversarial example. The computational efficiency is measured by the average time in generating an adversarial example. Experiments are conducted on an NVIDIA GeForce RTX 2080 GPU with 11GB of memory. The experimental results in Table 5 demonstrate that, although SEGA is not the most efficient attack method, it remains effective in generating adversarial examples, requiring only 1.3 seconds per example.

## 5 Conclusion and Discussion

Previous studies have highlighted the difficulty of transferring adversarial examples across NR-IQA models. In this work, we address this challenge by proposing SEGA, a transfer-based black-box attack method. SEGA uses Gaussian smoothing to reduce noises in the source model gradients and ensembles the smoothed gradients of multiple source models to approximate the target model gradient. Besides, SEGA incorporates a perturbation filtering module to remove inappropriate perturbations, thereby improving the imperceptibility of adversarial perturbations.

This work takes the first step in exploring transfer-based black-box attacks on NR-IQA models, revealing their vulnerability in black-box scenarios. It also highlights the critical role of smoothed gradient approximation in improving the transferability of adversarial examples. This work is limited by the trade-off between transferability, perturbation imperceptibility, and computational efficiency, as discussed in Sec. 4. Enhancing computational efficiency while maintaining the high transferability of SEGA will be the focus of our future work.

## References

- [1] Farhan Ullah, Bofeng Zhang, and Rehan Ullah Khan. Image-based service recommendation system: A JPEG-coefficient RFs approach. *IEEE Access*, 8:3308–3318, 2019.
- [2] Haoxuan Che, Siyu Chen, and Hao Chen. Image quality-aware diagnosis via meta-knowledge co-embedding. In *IEEE/CVF Conference on Computer Vision and Pattern Recognition*, pages 19819–19829, 2023.
- [3] Ce Zhang and Azim Eskandarian. A quality index metric and method for online self-assessment of autonomous vehicles sensory perception. *IEEE Transactions on Intelligent Transportation Systems*, 24(12):13801–13812, 2023.
- [4] Richard Zhang, Phillip Isola, Alexei A. Efros, Eli Shechtman, and Oliver Wang. The unreasonable effectiveness of deep features as a perceptual metric. In *IEEE/CVF Conference on Computer Vision and Pattern Recognition*, pages 586–595, 2018.
- [5] Keyan Ding, Kede Ma, Shiqi Wang, and Eero P. Simoncelli. Image quality assessment: Unifying structure and texture similarity. *IEEE Transactions on Pattern Analysis and Machine Intelligence*, 44(5):2567–2581, 2022.
- [6] Sidi Yang, Tianhe Wu, Shuwei Shi, Shanshan Lao, Yuan Gong, Mingdeng Cao, Jiahao Wang, and Yujiu Yang. MANIQA: Multi-dimension attention network for no-reference image quality assessment. In *IEEE/CVF Conference on Computer Vision and Pattern Recognition Workshop*, pages 1190–1199, 2022.
- [7] Weixia Zhang, Kede Ma, Jia Yan, Dexiang Deng, and Zhou Wang. Blind image quality assessment using a deep bilinear convolutional neural network. *IEEE Transactions on Circuits and Systems for Video Technology*, 30(1):36–47, 2020.
- [8] Kede Ma, Zhengfang Duanmu, Qingbo Wu, Zhou Wang, Hongwei Yong, Hongliang Li, and Lei Zhang. Waterloo exploration database: New challenges for image quality assessment models. *IEEE Transactions on Image Processing*, 26(2):1004–1016, 2017.
- [9] Weixia Zhang, Dingquan Li, Xiongkuo Min, Guangtao Zhai, Guodong Guo, Xiaokang Yang, and Kede Ma. Perceptual attacks of no-reference image quality models with human-in-the-loop. In *Annual Conference on Neural Information Processing Systems*, pages 2916–2929, 2022.
- [10] Ekaterina Shumitskaya, Anastasia Antsiferova, and Dmitriy S. Vatolin. Universal perturbation attack on differentiable no-reference image- and video-quality metrics. In *British Machine Vision Conference*, pages 1–12, 2022.
- [11] Chenxi Yang, Yujia Liu, Dingquan Li, and Tingting Jiang. Exploring vulnerabilities of no-reference image quality assessment models: A query-based black-box method. *IEEE Transactions on Circuits and Systems for Video Technology*, 34(12):12715–12729, 2024.

- [12] S. Alireza Golestaneh, Saba Dadsetan, and Kris M. Kitani. No-reference image quality assessment via transformers, relative ranking, and self-consistency. In *IEEE/CVF Winter Conference on Applications of Computer Vision*, pages 3989–3999, 2022.
- [13] Michele A. Saad, Margaret H. Pinson, David G. Nicholas, Niels Van Kets, Glenn Van Wallendael, Ramesh Jaladi, and Philip J. Corriveau. Image quality of experience: A subjective test targeting the consumer’s experience. In *Human Vision and Electronic Imaging*, pages 1–6, 2016.
- [14] American College of Radiology. Detecting image quality in medical imaging, 2024.
- [15] Ekaterina Shumitskaya, Anastasia Antsiferova, and Dmitriy Vatolin. Towards adversarial robustness verification of no-reference image-and video-quality metrics. *Computer Vision and Image Understanding*, 240:103913, 2024.
- [16] Ekaterina Shumitskaya, Anastasia Antsiferova, and Dmitriy Vatolin. IOI: Invisible one-iteration adversarial attack on no-reference image-and video-quality metrics. In *International Conference on Machine Learning*, pages 1–24, 2024.
- [17] Yujia Liu, Chenxi Yang, Dingquan Li, Jianhao Ding, and Tingting Jiang. Defense against adversarial attacks on no-reference image quality models with gradient norm regularization. In *IEEE/CVF Conference on Computer Vision and Pattern Recognition*, pages 25554–25563, 2024.
- [18] Daniel Smilkov, Nikhil Thorat, Been Kim, Fernanda Viégas, and Martin Wattenberg. SmoothGrad: Removing noise by adding noise. *arXiv preprint arXiv:1706.03825*, 2017.
- [19] David Balduzzi, Marcus Frean, Lennox Leary, JP Lewis, Kurt Wan-Duo Ma, and Brian McWilliams. The shattered gradients problem: If resnets are the answer, then what is the question? In *International Conference on Machine Learning*, pages 342–350, 2017.
- [20] Yinpeng Dong, Fangzhou Liao, Tianyu Pang, Hang Su, Jun Zhu, Xiaolin Hu, and Jianguo Li. Boosting adversarial attacks with momentum. In *IEEE/CVF Conference on Computer Vision and Pattern Recognition*, pages 9185–9193, 2018.
- [21] Deepti Ghadiyaram and Alan C. Bovik. Massive online crowdsourced study of subjective and objective picture quality. *IEEE Transactions on Image Processing*, 25(1):372–387, 2016.
- [22] Ian J. Goodfellow, Jonathon Shlens, and Christian Szegedy. Explaining and harnessing adversarial examples. In *International Conference on Learning Representations*, pages 1–11, 2015.
- [23] Thibault Maho, Teddy Furon, and Erwan Le Merrer. SurFree: A fast surrogate-free black-box attack. In *IEEE/CVF Conference on Computer Vision and Pattern Recognition*, pages 10430–10439, 2021.
- [24] Yu Ran, Ao-Xiang Zhang, Mingjie Li, Weixuan Tang, and Yuan-Gen Wang. Black-box adversarial attacks against image quality assessment models. *Expert Systems with Applications*, 260:125415, 2025.
- [25] Nathan Inkawich, Wei Wen, Hai (Helen) Li, and Yiran Chen. Feature space perturbations yield more transferable adversarial examples. In *IEEE/CVF Conference on Computer Vision and Pattern Recognition*, pages 7066–7074, 2019.
- [26] Yujia Liu, Ming Jiang, and Tingting Jiang. Transferable adversarial examples based on global smooth perturbations. *Computers & Security*, 121:1–10, 2022.
- [27] Jari Korhonen and Junyong You. Adversarial attacks against blind image quality assessment models. In *the 2nd Workshop on Quality of Experience in Visual Multimedia Applications*, pages 3–11, 2022.
- [28] Kaiming He, Xiangyu Zhang, Shaoqing Ren, and Jian Sun. Deep residual learning for image recognition. In *IEEE/CVF Conference on Computer Vision and Pattern Recognition*, pages 770–778, 2016.

[29] Florian Tramèr, Nicolas Papernot, Ian Goodfellow, Dan Boneh, and Patrick McDaniel. The space of transferable adversarial examples. *arXiv preprint arXiv:1704.03453*, 2017.

[30] Lei Wu, Zhanxing Zhu, Cheng Tai, and E Weinan. Understanding and enhancing the transferability of adversarial examples. *arXiv preprint arXiv:1802.09707*, 2018.

[31] Andrew Starnes, Anton Dereventsov, and Clayton Webster. Gaussian smoothing gradient descent for minimizing high-dimensional non-convex functions. *arXiv preprint arXiv:2311.00521*, 2023.

[32] Jiadong Lin, Chuanbiao Song, Kun He, Liwei Wang, and John E. Hopcroft. Nesterov accelerated gradient and scale invariance for adversarial attacks. In *International Conference on Learning Representations*, pages 1–12, 2020.

[33] Pascal Sebah and Xavier Gourdon. Introduction to the gamma function. *American Journal of Scientific Research*, pages 2–18, 2002.

[34] Honghai Yu and Stefan Winkler. Image complexity and spatial information. In *International Conference on Quality of Multimedia Experience*, pages 12–17, 2013.

[35] Anmin Liu, Weisi Lin, Manoranjan Paul, Chenwei Deng, and Fan Zhang. Just noticeable difference for images with decomposition model for separating edge and textured regions. *IEEE Transactions on Circuits and Systems for Video Technology*, 20(11):1648–1652, 2010.

[36] Shaolin Su, Qingsen Yan, Yu Zhu, Cheng Zhang, Xin Ge, Jinqiu Sun, and Yanning Zhang. Blindly assess image quality in the wild guided by a self-adaptive hyper network. In *IEEE/CVF Conference on Computer Vision and Pattern Recognition*, pages 3664–3673, 2020.

[37] Dingquan Li, Tingting Jiang, and Ming Jiang. Norm-in-norm loss with faster convergence and better performance for image quality assessment. In *ACM International Conference on Multimedia*, pages 789–797, 2020.

[38] Weixia Zhang, Guangtao Zhai, Ying Wei, Xiaokang Yang, and Kede Ma. Blind image quality assessment via vision-language correspondence: A multitask learning perspective. In *IEEE/CVF Conference on Computer Vision and Pattern Recognition*, pages 14071–14081, 2023.

[39] Zhou Wang, Alan C. Bovik, Hamid R. Sheikh, and Eero P. Simoncelli. Image quality assessment: From error visibility to structural similarity. *IEEE Transactions on Image Processing*, 13(4):600–12, 2004.

[40] Albert S. Berahas, Liyuan Cao, Krzysztof Choromanski, and Katya Scheinberg. A theoretical and empirical comparison of gradient approximations in derivative-free optimization. *Foundations of Computational Mathematics*, 22(2):507–560, 2022.

[41] Pin-Yu Chen, Huan Zhang, Yash Sharma, Jinfeng Yi, and Cho-Jui Hsieh. ZOO: Zeroth order optimization based black-box attacks to deep neural networks without training substitute models. In *ACM Workshop on Artificial Intelligence and Security*, pages 15–26, 2017.

[42] Nathan Inkawich, Kevin J. Liang, Binghui Wang, Matthew Inkawich, Lawrence Carin, and Yiran Chen. Perturbing across the feature hierarchy to improve standard and strict blackbox attack transferability. In *Annual Conference on Neural Information Processing Systems*, pages 1–11, 2020.

## Appendix

### A Proof of Theorem 1

**Theorem 1** Suppose  $f$  is Lipschitz-continuous, and  $f_\sigma$  is the Gaussian smoothing of  $f$ . Then, for every  $x$ , we have

$$\lim_{\sigma \rightarrow 0} f_\sigma(x) = f(x). \quad (14)$$

**Proof:** Suppose  $f$  is Lipschitz-continuous with  $L$  as the Lipschitz constant. Recall that

$$f_\sigma(x) = \frac{1}{(2\pi)^{d/2}} \int_{\mathbb{R}^d} f(x + \sigma u) e^{-\|u\|_2^2/2} du, \quad (15)$$

so

$$\begin{aligned} |f_\sigma(x) - f(x)| &= \left| \frac{1}{(2\pi)^{d/2}} \int_{\mathbb{R}^d} (f(x + \sigma u) - f(x)) e^{-\|u\|_2^2/2} du \right| \\ &\leq \frac{1}{(2\pi)^{d/2}} \int_{\mathbb{R}^d} |f(x + \sigma u) - f(x)| e^{-\|u\|_2^2/2} du. \end{aligned} \quad (16)$$

Since  $f$  is Lipschitz-continuous, we have

$$|f(x + \sigma u) - f(x)| \leq L\|\sigma u\|. \quad (17)$$

Therefore,

$$\begin{aligned} |f_\sigma(x) - f(x)| &\leq \frac{L \cdot \sigma}{(2\pi)^{d/2}} \int_{\mathbb{R}^d} \|u\| e^{-\|u\|_2^2/2} du \\ &= (L \cdot \sigma) \mathbb{E}_{u \sim \mathcal{N}(0, I_d)} [\|u\|]. \end{aligned} \quad (18)$$

Since  $u_i \sim \mathcal{N}(0, 1)$ , we have  $u_i^2 \sim \chi^2(1)$ . Therefore,  $\sum_{i=1}^d u_i^2 \sim \chi^2(d)$ , i.e.

$$\|u\|_2^2 \sim \chi^2(d). \quad (19)$$

Let the variables be defined as  $Y = \|u\|_2^2$  and  $V = \|u\|$ . Using the transformation technique with  $V = g(Y) = \sqrt{Y}$ , the probability density function of  $V$  is given by

$$f_V(v) = f_Y(g^{-1}(y)) \left| \frac{dy}{dv} \right| = \frac{y^{d-1} e^{-y^2/2}}{2^{d/2-1} \Gamma(\frac{d}{2})}, \quad y > 0. \quad (20)$$

Therefore, the expectation of  $V = \|u\|$  is

$$\mathbb{E}_{u \sim \mathcal{N}(0, I_d)} [\|u\|] = \int_0^\infty \frac{y^d e^{-y^2/2}}{2^{d/2-1} \Gamma(\frac{d}{2})} dy = \sqrt{2} \frac{\Gamma(\frac{d+1}{2})}{\Gamma(\frac{d}{2})}. \quad (21)$$

Therefore,

$$|f_\sigma(x) - f(x)| \leq (L \cdot \sigma) \mathbb{E}_{u \sim \mathcal{N}(0, I_d)} [\|u\|] = (L \cdot \sigma) \sqrt{2} \frac{\Gamma(\frac{d+1}{2})}{\Gamma(\frac{d}{2})}. \quad (22)$$

Let  $\sigma \rightarrow 0$  in Eq. (22), we have

$$\lim_{\sigma \rightarrow 0} |f_\sigma(x) - f(x)| = 0. \quad (23)$$

Thus, we have proved

$$\lim_{\sigma \rightarrow 0} f_\sigma(x) = f(x). \quad (24)$$

□

## B Proof of Theorem 2

**Theorem 2** Suppose the gradient of the target model  $h$  is  $L$ -Lipschitz with  $L$  being the Lipschitz constant, and  $\hat{g}(x)$  is defined as

$$\hat{g}(x) = \frac{1}{K} \sum_{k=1}^K \nabla f_\sigma^k(x), \quad (25)$$

we have

$$\|\hat{g}(x) - \nabla h(x)\| \leq \left( L\sigma + \frac{C}{\sigma} \right) \sqrt{2} \frac{\Gamma(\frac{d+1}{2})}{\Gamma(\frac{d}{2})}, \quad (26)$$

where  $C$  is a constant related to  $\{f^1, \dots, f^K\}$  and  $\Gamma(\cdot)$  represents the Gamma function [33].

**Proof:** Suppose  $\nabla h(x)$  is Lipschitz-continuous with  $L$  as the Lipschitz constant. According to work [40],

$$\nabla f_\sigma(x) = \frac{1}{\sigma} \mathbb{E}_{u \sim \mathcal{N}(0, I_d)} [f(x + \sigma u)u]. \quad (27)$$

Moreover, each source model  $f^k \in \{f^1, \dots, f^K\}$  can be represented by

$$f^k(x) = h(x) + \varepsilon^k(x), \quad (28)$$

where  $\varepsilon^k(x)$  is the error function. Assume the absolute value of each  $\varepsilon^k(x)$  is bounded by a constant  $c^k$ , i.e.  $|\varepsilon^k(x)| \leq c^k$ . Let  $C = \max\{c^1, \dots, c^K\}$ .

Recall that

$$\hat{g}(x) = \frac{1}{K} \sum_{k=1}^K \nabla f_\sigma^k(x), \quad (29)$$

then

$$\begin{aligned} \|\hat{g}(x) - \nabla h(x)\| &= \left\| \frac{1}{K \cdot \sigma} \sum_{k=1}^K \mathbb{E}[f^k(x + \sigma u)u] - \nabla h(x) \right\| \\ &= \left\| \frac{1}{K} \sum_{k=1}^K (\mathbb{E}[h(x + \sigma u)u/\sigma] + \mathbb{E}[\varepsilon^k(x + \sigma u)u/\sigma]) - \nabla h(x) \right\| \\ &= \left\| \frac{1}{K} \sum_{k=1}^K \mathbb{E}[\nabla h(x + \sigma u) - \nabla h(x)] + \frac{1}{K} \sum_{k=1}^K \mathbb{E} \left[ \frac{\varepsilon^k(x + \sigma u)u}{\sigma} \right] \right\| \\ &\leq \frac{1}{K} \sum_{k=1}^K \mathbb{E} \|\nabla h(x + \sigma u) - \nabla h(x)\| + \frac{1}{K} \sum_{k=1}^K \mathbb{E} \left\| \frac{\varepsilon^k(x + \sigma u)u}{\sigma} \right\| \\ &\leq \frac{L \cdot \sigma}{K} \sum_{k=1}^K \mathbb{E} \|u\| + \frac{C}{K \cdot \sigma} \sum_{k=1}^K \mathbb{E} \|u\| \\ &= \left( L\sigma + \frac{C}{\sigma} \right) \mathbb{E} \|u\| = \left( L\sigma + \frac{C}{\sigma} \right) \sqrt{2} \frac{\Gamma(\frac{d+1}{2})}{\Gamma(\frac{d}{2})}. \end{aligned} \quad (30)$$

□

## C The Overall Algorithm of SEGA

The overall algorithm of SEGA is shown in Alg. 1.

## D Experimental Details

**Training details.** This section provides the training details of the NR-IQA models used in the main experiments. All experiments were conducted on the widely used LIVEC dataset [21], with 80% of the images randomly selected for training and the remaining 20% reserved for evaluating adversarial attacks. This data split follows the protocol adopted in [17].

---

**Algorithm 1** Signed Ensemble Gaussian Attack (SEGA)

---

**Inputs:** Source models  $f^1, \dots, f^K$ , target model  $h$ , original image  $x$ , JND mask  $JND(x)$   
**Parameters:** A pre-defined threshold  $\alpha$ , attack strength  $\epsilon$ , Gaussian smoothing parameter  $\sigma$ , sampling number  $m$   
**Output:** Adversarial example  $\tilde{x}$

```
1: Initialize  $\hat{g} \leftarrow 0$ 
2: for  $k = 1$  to  $K$  do
3:   for  $i = 1$  to  $m$  do
4:      $\hat{g} \leftarrow \hat{g} + \nabla f^k(x + \sigma u_i^k)$ , where  $u_i^k \sim \mathcal{N}(0, I_d)$ .
5:   end for
6: end for
7:  $\hat{g} \leftarrow \hat{g}/Km$ 
8:  $M^{\mathcal{F}} \leftarrow \hat{g} \geq \alpha$  {See Eq. (11)}
9:  $M^{JND} \leftarrow JND(x) \geq \epsilon$  {See Eq. (12)}
10: if  $h(x)$  is high then
11:    $\tilde{x} \leftarrow x - M^{JND} \odot M^{\mathcal{F}} \odot (\epsilon \cdot \text{sgn}(\hat{g}))$  {decrease score}
12: else
13:    $\tilde{x} \leftarrow x + M^{JND} \odot M^{\mathcal{F}} \odot (\epsilon \cdot \text{sgn}(\hat{g}))$  {increase score}
14: end if
15: return  $\tilde{x}$ 
```

---

All NR-IQA models, including HyperIQA [36], DBCNN [7], LinearityIQA [37], LIQE [38], and MANIQ [6] are trained on the same training dataset using the official implementations released by their respective authors.

**Attack Details.** The one-step FGSM is implemented following the setup in [17]<sup>2</sup>, while the other attack methods use the official implementations released by their respective authors.

## E Image Quality of Adversarial Examples

Due to space limitations, we report only the SSIM values between adversarial examples and original images in Sec. 4.3. In this section, we provide a more comprehensive evaluation of the imperceptibility of adversarial perturbations. Table 6 includes four additional metrics: the  $\ell_2$  and  $\ell_\infty$  norms of the perturbations, as well as two widely-used full-reference IQA metrics, LPIPS [4] and DISTS [5], computed between the adversarial examples and the original images. Consistent with the main results, the source model used here is the one demonstrating the highest transferability to the target model.

Table 6 supports the conclusion presented in the main manuscript. Since SEGA is an  $\ell_\infty$ -bounded attack method, the  $\ell_\infty$  norm of the perturbation remains fixed for a given  $\epsilon$ . Notably, SEGA achieves the smallest  $\ell_2$  norm of perturbations compared with other methods. We attribute this to the perturbation filtering module, which results in many pixels receiving no perturbation. LPIPS and DISTS values exhibit a similar trend, collectively indicating that adversarial examples generated by SEGA have better image quality compared to those produced by FGSM [22] and OUAP [15]. It is interesting to note that Pattack [9] performs exceptionally well when evaluated using LPIPS but does not perform as well when measured by SSIM. This difference arises because LPIPS is used as an optimization constraint in Pattack, whereas SSIM is not. Based on LPIPS and DISTS values, we can roughly rank the attack methods in descending order of image quality for adversarial examples: Pattack > Kor [27] > IOI [16] > SEGA > FGSM > OUAP.

Additional visualization results are provided in Fig. 6, where a set of adversarial examples is shown for each target model. It is evident that the perturbations in adversarial examples generated by SEGA are difficult to detect, particularly in images with extensive low-frequency regions, such as Fig. 6 (d).

---

<sup>2</sup><https://github.com/Yangid/DefenseIQA-NT>

Table 6: Quantitative comparison of the image quality of adversarial examples generated by different attack methods against various target models.

attack	source	$\ell_\infty \downarrow$	$\ell_2 \downarrow$	SSIM $\uparrow$	LPIPS $\downarrow$	DISTS $\downarrow$
Target: HyperIQA						
FGSM	DBCNN	8	0.020	0.733	0.310	0.191
Pattack	Linearity	69.414	0.025	0.731	0.068	0.076
OUAP	Linearity	8	0.017	0.815	0.345	0.216
IOI	Linearity	33.522	0.016	0.883	0.203	0.154
Kor	-	39.185	0.016	0.931	0.185	0.149
SEGA	-	8	0.015	0.862	0.245	0.175
Target: DBCNN						
FGSM	LIQE	8	0.020	0.755	0.299	0.199
Pattack	Linearity	69.414	0.025	0.731	0.068	0.076
OUAP	LIQE	8	0.017	0.803	0.309	0.200
IOI	Linearity	33.522	0.016	0.883	0.203	0.154
Kor	-	39.185	0.016	0.931	0.185	0.149
SEGA	-	8	0.015	0.857	0.235	0.167
Target: LinearityIQA						
FGSM	HyperIQA	8	0.020	0.740	0.317	0.191
Pattack	HyperIQA	68.888	0.024	0.733	0.067	0.076
OUAP	DBCNN	8	0.015	0.826	0.343	0.222
IOI	HyperIQA	34.284	0.016	0.888	0.187	0.139
Kor	-	39.185	0.016	0.931	0.185	0.149
SEGA	-	8	0.014	0.881	0.228	0.167
Target: LIQE						
FGSM	HyperIQA	8	0.020	0.740	0.317	0.191
Pattack	HyperIQA	68.888	0.024	0.733	0.067	0.076
OUAP	DBCNN	8	0.015	0.826	0.343	0.222
IOI	HyperIQA	34.284	0.016	0.888	0.187	0.139
Kor	-	39.185	0.016	0.931	0.185	0.149
SEGA	-	8	0.015	0.863	0.247	0.174

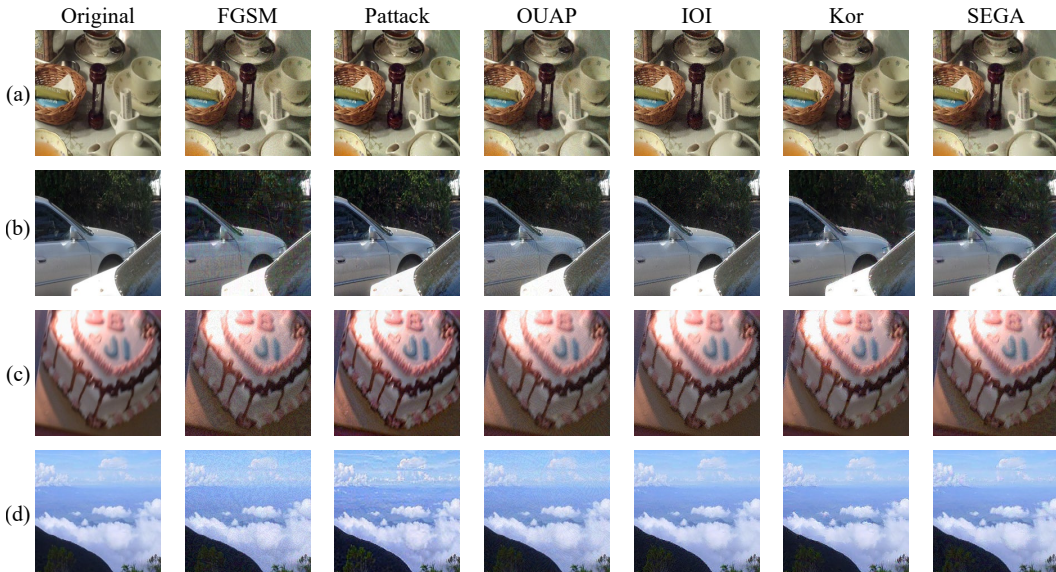


Figure 6: Visualization of adversarial examples generated by different attack methods against different target models, (a) HyperIQA, (b) DBCNN, (c) LinearityIQA, (d) LIQE. Please zoom in for a clearer view.

## F An Ensemble Strategy of Compared Methods

In Sec. 4.2 of the main manuscript, we report the best transferability results of the compared attacks across all source-target model pairs. In this section, we design an ensemble strategy for the compared methods, enabling them to utilize ensembled gradients in a way similar to SEGA.

Table 7: Comparison of SEGA with SOTA attack methods using the ensemble strategy.

Target: HyperIQA					Target: DBCNN						
	MAE $\uparrow$	R $\downarrow$	SROCC $\downarrow$	PLCC $\downarrow$	KROCC $\downarrow$		MAE $\uparrow$	R $\downarrow$	SROCC $\downarrow$	PLCC $\downarrow$	KROCC $\downarrow$
FGSM	8.929	1.024	0.840	0.855	0.664	7.166	1.071	0.866	0.861	0.682	
Ptack	7.375	1.167	0.959	0.948	0.834	5.058	1.279	0.974	0.975	0.870	
OUAP	4.205	1.498	0.965	0.954	0.848	2.912	1.548	0.978	0.975	0.869	
IOI	5.524	1.292	0.973	0.966	0.864	4.290	1.401	0.970	0.962	0.858	
Kor	<b>16.505</b>	<b>0.781</b>	0.858	0.842	0.675	8.914	1.028	0.883	0.869	0.710	
SEGA	12.186	0.883	<b>0.675</b>	<b>0.706</b>	<b>0.507</b>	<b>10.493</b>	<b>0.876</b>	<b>0.562</b>	<b>0.626</b>	<b>0.418</b>	
Target: LinearityIQA					Target: LIQE						
	MAE $\uparrow$	R $\downarrow$	SROCC $\downarrow$	PLCC $\downarrow$	KROCC $\downarrow$		MAE $\uparrow$	R $\downarrow$	SROCC $\downarrow$	PLCC $\downarrow$	KROCC $\downarrow$
FGSM	12.787	0.880	0.790	0.754	0.602	8.133	1.267	0.952	0.943	0.825	
Ptack	8.042	1.126	0.962	0.941	0.834	5.781	1.477	0.980	0.978	0.889	
OUAP	5.583	1.366	0.947	0.931	0.808	3.004	1.795	0.990	0.991	0.923	
IOI	7.114	1.210	0.946	0.935	0.811	5.102	1.689	0.979	0.973	0.896	
Kor	14.475	0.913	0.802	0.786	0.612	10.742	1.311	0.899	0.883	0.752	
SEGA	<b>17.938</b>	<b>0.700</b>	<b>0.504</b>	<b>0.503</b>	<b>0.366</b>	<b>15.094</b>	<b>0.927</b>	<b>0.831</b>	<b>0.801</b>	<b>0.663</b>	

Specifically, for each compared method, we compute the final adversarial examples by averaging the adversarial perturbations generated across all source models. For instance, if  $\Delta x_1$ ,  $\Delta x_2$ ,  $\Delta x_3$  are adversarial perturbations generated by FGSM against source model HyperIQA, DBCNN, and LIQE, respectively, the final adversarial image is given by:

$$x + \frac{\Delta x_1 + \Delta x_2 + \Delta x_3}{3}. \quad (31)$$

The set of source models includes {HyperIQA, DBCNN, LinearityIQA, LIQE}. When one model is selected as the target model, the remaining three are used as source models. The results are presented in Table 7.

SEGA consistently outperforms all compared methods in nearly all cases. For instance, when attacking DBCNN, only SEGA achieves an R robustness below 1. Additionally, the SROCC values of the compared methods remain above 0.85, indicating their limited effectiveness in disrupting prediction consistency. In contrast, SEGA achieves an SROCC of 0.5622, demonstrating its strong capability in effectively attacking the target DBCNN model. Furthermore, SEGA maintains strong transferability across all metrics regardless of the target model, whereas the transferability of the compared methods is inconsistent. For example, the Kor attack demonstrates good transferability in terms of R robustness when attacking HyperIQA and LinearityIQA but performs poorly when attacking DBCNN and LIQE.

The experimental results highlight the superiority of SEGA, even when the compared methods also employ the ensemble strategy. This demonstrates the effectiveness of combining Gaussian smoothing, gradient ensembling, and perturbation filtering in SEGA to achieve enhanced transferability.

## G Ablation Studies

**Ablation study of  $\alpha$  in perturbation filtering.** Following the ablation study setup in Sec. 4.4, this experiment is conducted using DBCNN as the target model. The filtering of inappropriate perturbations based on the JND mask is retained, while the threshold  $\alpha$  in Eq. (11) is varied. A larger value of  $\alpha$  indicates that more gradient components are considered unimportant and thus removed during perturbation filtering.

The results are presented in Fig. 7, where the left subfigure illustrates the attack performance and the right shows the imperceptibility of adversarial perturbations, measured by SSIM and LPIPS. It can be observed that the threshold  $\alpha$  influences the trade-off between attack effectiveness and imperceptibility. Specifically, larger values of  $\alpha$  lead to improved imperceptibility but reduced attack success.

This is intuitively reasonable. According to Eq. (11), increasing  $\alpha$  causes more components in  $\mathcal{F}(\hat{g})$  to be set to zero, resulting in smaller perturbations that are less perceptible but also less effective in misleading the model. In the main experiments, we set  $\alpha = 0.02$ .

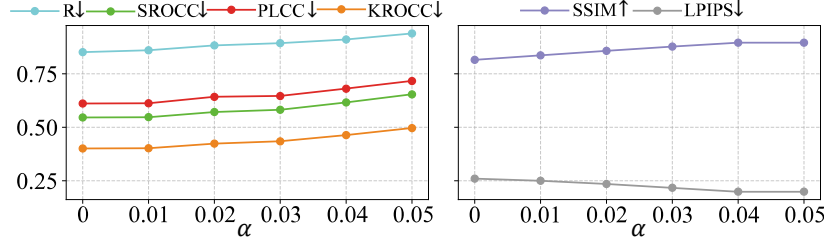


Figure 7: Ablation study of gradient filtering parameter  $\alpha$ .

## H SEGA Under Defense Strategies

In this section, we evaluate the transferability of SEGA under a defense strategy. Recently, Liu *et al.* [17] proposed a Norm regularization Training (NT) strategy for enhancing the robustness of NR-IQA models by incorporating gradient norm regularization into the loss function. Following the training settings outlined in their work [17], we use the NT strategy and train HyperIQA-NT, DBCNN-NT, LinearityIQA-NT, LIQE-NT models with the regularization weight set to 0.0005. For simplicity of comparison, we apply the ensemble strategy introduced in the previous section to FGSM, Pattack, OUAP, and IOI, and present the comparison results in Table 8.

Table 8: Attack performance of attack methods against robustly trained NR-IQA models.

	Target: HyperIQA-NT					Target: DBCNN-NT				
	MAE $\uparrow$	$R \downarrow$	$SROCC \downarrow$	$PLCC \downarrow$	$KROCC \downarrow$	MAE $\uparrow$	$R \downarrow$	$SROCC \downarrow$	$PLCC \downarrow$	$KROCC \downarrow$
FGSM	2.507	1.745	0.987	0.981	0.908	4.160	1.354	0.946	0.940	0.801
Pattack	5.730	1.229	0.968	0.960	0.852	4.135	1.466	0.978	0.966	0.871
OUAP	2.057	1.730	0.992	0.990	0.931	1.968	1.774	0.981	0.983	0.884
IOI	2.741	1.585	0.985	0.985	0.913	2.659	1.664	0.981	0.975	0.883
Kor	<b>8.013</b>	<b>1.129</b>	<b>0.894</b>	<b>0.894</b>	<b>0.741</b>	<b>7.601</b>	<b>1.159</b>	0.927	0.894	0.769
SEGA	5.054	1.515	0.924	0.917	0.793	6.556	1.171	<b>0.834</b>	<b>0.817</b>	<b>0.659</b>

	Target: LinearityIQA-NT					Target: LIQE-NT				
	MAE $\uparrow$	$R \downarrow$	$SROCC \downarrow$	$PLCC \downarrow$	$KROCC \downarrow$	MAE $\uparrow$	$R \downarrow$	$SROCC \downarrow$	$PLCC \downarrow$	$KROCC \downarrow$
FGSM	11.240	0.960	0.820	0.821	0.633	9.828	1.104	0.974	0.963	0.869
Pattack	7.016	1.218	0.958	0.959	0.836	7.231	1.217	0.987	0.984	0.908
OUAP	4.775	1.378	0.956	0.960	0.825	4.934	1.395	0.993	0.991	0.934
IOI	5.890	1.278	0.959	0.957	0.833	3.365	1.589	0.991	0.992	0.931
Kor	10.872	1.064	0.852	0.836	0.671	8.461	1.331	0.937	0.929	0.815
SEGA	<b>15.920</b>	<b>0.734</b>	<b>0.625</b>	<b>0.645</b>	<b>0.456</b>	<b>11.367</b>	<b>1.076</b>	<b>0.899</b>	<b>0.902</b>	<b>0.749</b>

Two key observations can be made from Table 8. Firstly, SEGA outperforms other attacks under the NT defense strategy in most cases, except when attacking HyperIQA-NT. While the compared methods almost lose their attack effectiveness against NT-trained models, SEGA demonstrates strong transferability against LinearityIQA-NT. Additionally, the MAE value achieved by SEGA against LIQE-NT is also satisfactory. Secondly, compared to the results reported in Table 7, the NT strategy significantly weakens the attack capability of all attacks. This phenomenon demonstrates

the effectiveness of NT in enhancing the robustness of NR-IQA models. On the other hand, it also highlights the need to design stronger attacks against robust models.

## I Comparison with Query-Based Attacks

Transfer-based attacks and query-based attacks are not directly comparable, as each has its own strengths. Transfer-based attacks are more time-efficient, while query-based attacks achieve better performance in black-box scenarios. This distinction has been demonstrated in several studies on attacks against image classification models [41]. Therefore, they are typically not compared directly within a single study on attacks against image classification models [26, 42].

Despite this, we still compare our method, SEGA, with the IQA-specific query-based attack proposed by Yang *et al.* [11] (denoted as SurFree-QA) to further demonstrate the effectiveness of SEGA. The results against DBCNN are shown in Table 9. As seen, SEGA outperforms SurFree-QA across all metrics, indicating that SEGA not only achieves better attack performance but is also more time-efficient. Specifically, the R robustness value drops below 0.9 when attacked by SEGA, whereas it remains around 1.4 when attacked by SurFree-QA. In addition to prediction accuracy, the robustness of prediction consistency follows a similar trend. SurFree-QA reduces the SROCC between predicted scores before and after the attack to 0.8397, while SEGA causes a more significant decrease, reducing it to 0.5622. Moreover, SEGA requires only 1.3 seconds to generate a single adversarial example, while SurFree-QA takes nearly 29 seconds for the same task. These experimental results demonstrate that SEGA is both an effective and efficient black-box attack method.

Table 9: Comparison of SEGA with IQA-specific query-based attack proposed by Yang *et al.*

method	SurFree-QA	SEGA
MAE $\uparrow$	5.974	<b>10.493</b>
R $\downarrow$	1.431	<b>0.876</b>
SROCC $\downarrow$	0.840	<b>0.562</b>
PLCC $\downarrow$	0.827	<b>0.626</b>
KROCC $\downarrow$	0.672	<b>0.418</b>
time(s) $\downarrow$	28.913	<b>1.310</b>